Int J Adv Manuf Technol (2010) 48:1–10
DOI 10.1007/s00170-009-2262-x

ORIGINAL ARTICLE

Spindle vibration suppression for advanced milling process by using self-tuning feedback control

Nan-Chyuan Tsai · Li-Wen Shih · Rong-Mao Lee

Received: 17 March 2009 / Accepted: 5 August 2009 / Published online: 20 August 2009

Abstract The goal of this work is to concurrently counterbalance the dynamic cutting force and regulate the spindle position deviation under various milling conditions by integrating active magnetic bearing (AMB) technique, fuzzy logic algorithm, and an adaptive self-tuning feedback loop. The experimental data, either for idle or cutting, are utilized to establish the database of milling dynamics so that the system parameters can be on-line estimated by employing the proposed fuzzy logic algorithm as the cutting mission is engaged. Based on the estimated milling system model and preset operation conditions, i.e., spindle speed, cut depth, and feed rate, the current cutting force can be numerically estimated. Once the current cutting force can be real time estimated, the corresponding compensation force can be exerted by the equipped AMB to counterbalance the cutting force, in addition to the spindle position regulation by feedback of spindle position. At the end, the experimental simulations on realistic milling are presented to verify the efficacy of the fuzzy controller for spindle position regulation and the capability of the dynamic cutting force counterbalance.

Keywords Active magnetic bearing · Cutting process · Fuzzy logic algorithm

N.-C. Tsai (✉) · L.-W. Shih · R.-M. Lee
Department of Mechanical Engineering,
National Cheng Kung University,
Tainan City 70101, Taiwan
e-mail: nortren@mail.ncku.edu.tw

1 Introduction

A few serious issues for high-speed milling, such as gyroscopic effect, severe chatter, high temperature, and potential crack growth inside cutters, still remain unsolved after decades of manufacturing technology evolution [1]. For the advanced milling systems in which magnetic bearings are embedded, although the upper limit of spindle speed is much increased to 10,000 rpm or above, yet the mathematic model of cutting process, to be used for prevention of high frequency vibration and chatter, becomes more complicated and inaccurate. In addition, the uncertainties of the metal cutting system and any potential unexpected disturbance, due to high-speed metal cutting, can also deteriorate the performance and stability of milling machines. Therefore, in this paper, a fuzzy second-order model for milling process by realistic experiments is constructed so that the self-tuning adaptive control algorithm and a set of active magnetic bearing (AMB) can be applied to counterbalance the cutting force, in addition to regulating the spindle position deviation.

In past two decades, numerous researches were devoted to construction of milling dynamics and control strategies in order to improve the quality of metal cutting and enhance the stability of mass production. For example, Lauderbaugh and Ulsoy reported an approach to model milling dynamics for various cut depths and spindle speeds [2]. Li et al. proposed a predictive time-domain mathematical model to determine the milling dynamics [3]. Besides, the first- and second-order mathematic models for milling process were ever proposed in 2001 and 2004, respectively [4, 5]. As for control loop design, a fast adaptive controller was presented to regulate the cutting force via feed rate tuning [6]. Similarly, an adaptive fuzzy logic controller was employed

to ensure stability robustness of milling systems against external disturbance [7]. In addition, an adaptive controller based on neural network was proposed to enhance the robustness and global stability of milling system [8].

The AMB technology is gradually applied in industries because it can operate with free mechanical friction against the spinning rotor. In 2002, Spirig et al. ever utilized a set of AMB to three types of revolving machines and analyzed the dynamics of spindles [9]. Moreover, AMBs were adopted by Kyung and Lee to attenuate chatter during milling process [10]. Although a conventional proportional–integral–derivative (PID) controller can be designed for AMBs to regulate spindle position deviation in most occasions [11], yet for high-speed milling, the PID controllers are not always applicable, either for stability or performance. Based on this argument, an advanced H^{∞} controller was ever proposed by Tsai et al. for high-speed rotor/AMB applications [12].

To much improve surface finish for the workpieces, a compact and low-cost module of AMB is employed in our work to concurrently counterbalance the cutting force and regulate spindle position under the proposed adaptive control strategies and estimation of cutting force. By the end, the efficacy of the AMB equipped at the milling machine is verified by intensive milling experiments.

2 Nonlinearity of the magnetic force by an AMB

The block diagram of the milling process aided by AMB is shown in Fig. 1, where the cutting force, F_c, is usually varying during milling operation and results in the position deviation of spindle, d. Therefore, the magnetic force, F_m, is proposed as the compensatory force to regulate the spindle position via an AMB as long as the position deviation of spindle and cutting force can be measured and estimated on-line, respectively. In Fig. 1, "i" is the coil current fed into the AMB. Since the magnetic force is highly nonlinear in terms of air gap and supplied current, the characteristics of magnetic force has to be explored at first before any control strategy is formulated.

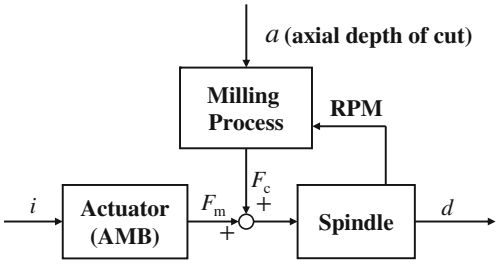

Fig. 1 Block diagram of milling process aided by AMB

The schematic design of four-pole AMB is depicted in Fig. 2. The average magnetic flux density for the presented pole profile design is increased by 11%, compared with the traditional rectangular pole design [13]. An auxiliary bush that has a maximum air gap, 0.5 mm, against the spindle is equipped by the free end of the spindle. Since the required magnetic force is function of coil current and the air gap between the rotor and magnetic pole [14], the experiments are designed and undertaken to unveil their relation. The test rig is schematically shown in Fig. 3. Control current for each pair of poles is applied to the coil via the signal processing interface, Module DS1104 by dSPACE, and a set of amplifier. Once the magnetic force is induced by the coil current, it can be measured by the load cell unit (Model: STC-25, by Accusys Technology Incorporation), shown in Fig. 4. A set of experimental results on magnetic force measurement, i.e., magnetic force versus current, are recorded and shown in Fig. 5.

Since the AMB is employed to provide the magnetic force to counterbalance the cutting force, the required coil current, i, can be calculated in terms of required magnetic force, F_m, and air gap, x, as follows:

$$i(F_m, x) = b_1 F_m^{4/5} + b_2 F_m^{11/5} + b_3 x^{-2/5} F_m^{6/5} + b_4 x^{-6/5} + b_5 x^{-13/5} + b_6 \quad (1)$$

where the coefficients $b_1 \sim b_6$ are constants obtained from curve fitting:

$$\begin{bmatrix} b_1 \\ b_2 \\ b_3 \\ b_4 \\ b_5 \\ b_6 \end{bmatrix} = \begin{bmatrix} 0.37803 \\ 0.00046 \\ -0.0801 \\ -1.3847 \\ 0.69404 \\ 0.64977 \end{bmatrix}. \quad (2)$$

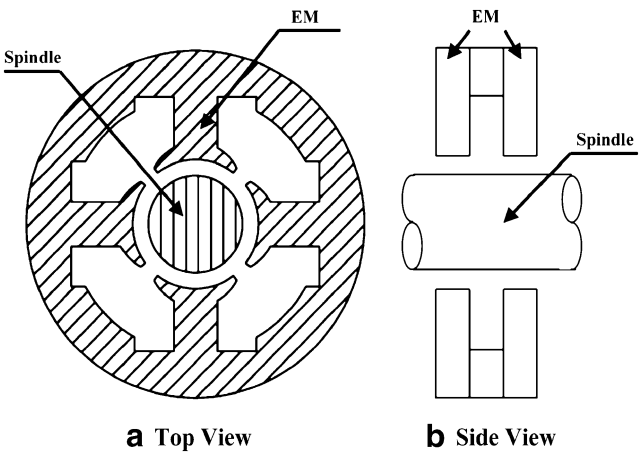

Fig. 2 Schematic design of four-pole AMB: **a** top view and **b** side view

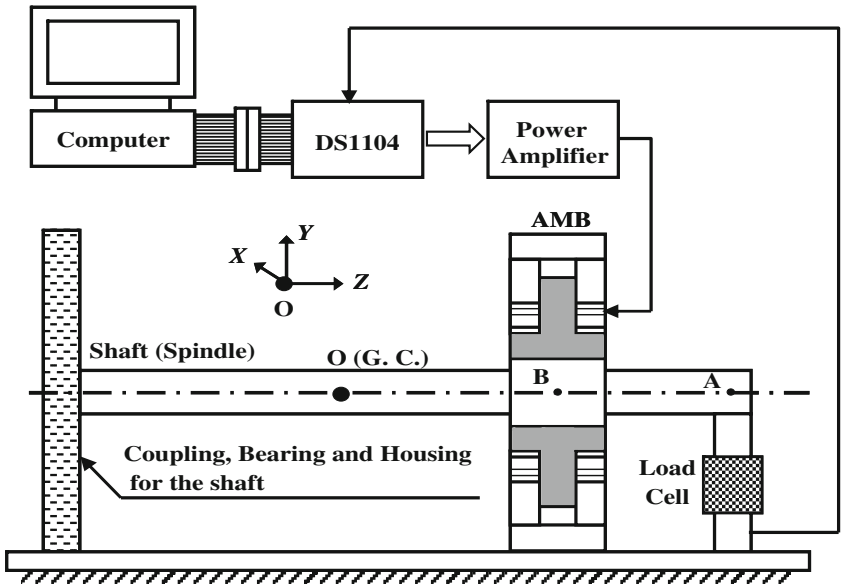

Fig. 3 Test rig of magnetic force measurement

3 Modeling of the spindle and cutting dynamics

For the milling process aided by AMB, shown in Fig. 1, the cutting force, F_c, is mainly determined by the axial cut depth, a, feed rate, f, and spindle speed, Ω. However, at normal operation mode, the spindle speed and feed rate are generally retained constants. Therefore, the axial cut depth, a, is, in fact, the key factor to determine the pattern of cutting dynamics. In order to counterbalance the cutting force and regulate the spindle position deviation, d, the models of the subsystems, shown in Fig. 6, are to be constructed by experiments at first.

In Fig. 6a, the lateral force to the spindle, F_m, represents the magnetic force exerting on the spindle by the AMB while the cutting process is not engaged at all. The spindle model at idle operation mode, shown in Fig. 6a, is constructed in order to explore the link of the shaft position deviation, d, against the corresponding exerted force, i.e., the magnetic force, F_m. Similarly, the dynamic model shown in Fig. 6b represents the spindle position deviation, d, against the axial cut depth, a. By comparison of the two dynamic models in Fig. 6, the resulted cutting force, due to milling process, can be estimated for a given axial cut depth and the available measurement of spindle position.

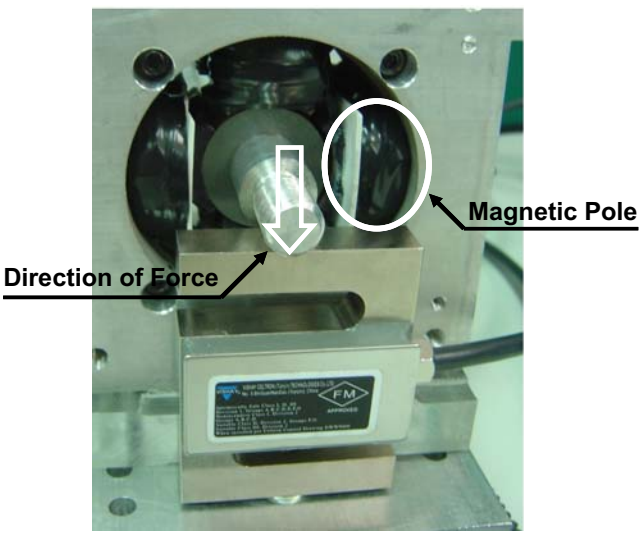

Fig. 4 Photo of magnetic force measurement

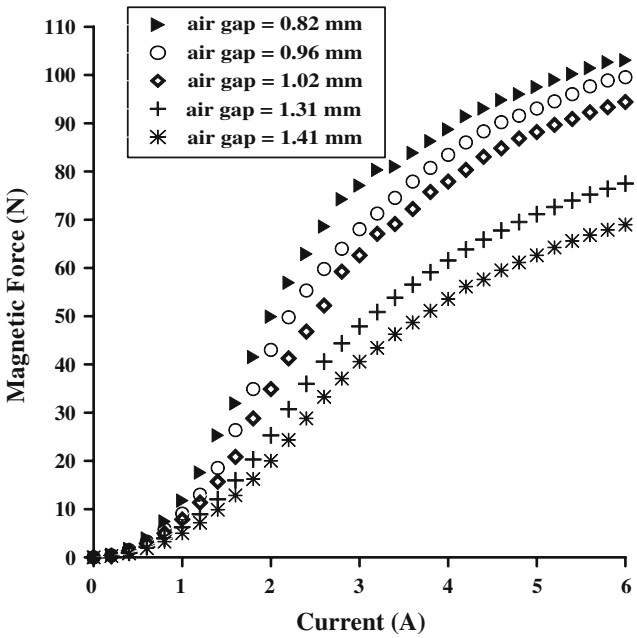

Fig. 5 Magnetic force versus coil current

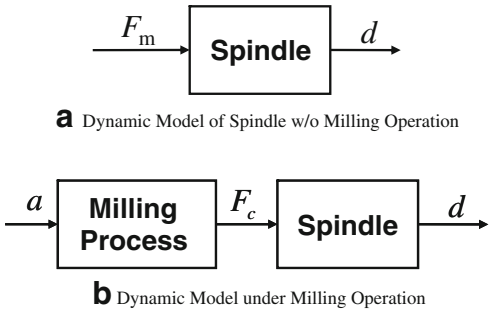

Fig. 6 Dynamic model to approximate milling process. **a** Dynamic model of spindle without milling operation. **b** Dynamic model under milling operation

3.1 Modeling of spindle dynamics

In this paper, an AMB is employed to provide the magnetic force, F_m, to regulate the position deviation of spindle, d. Therefore, the transfer function of spindle dynamics can be represented as follows:

$$\begin{bmatrix} d_x \\ d_y \end{bmatrix} = G^u(s) \begin{bmatrix} F_{mx} \\ F_{my} \end{bmatrix} = \begin{bmatrix} G^u_{xx}(s) & G^u_{xy}(s) \\ G^u_{yx}(s) & G^u_{yy}(s) \end{bmatrix} \begin{bmatrix} F_{mx} \\ F_{my} \end{bmatrix} \quad (3)$$

where the spindle position deviation, d, is decomposed into the components d_x and d_y in X- and Y-axes, respectively, and so is the magnetic force, F_m. $G^u(s)$ is the transfer function of spindle dynamics at idle operation mode. $G^u_{ij}(s)(i = x, y;\ j = x, y)$ represents the individual transfer function for the system output, d_i, with respect to the input, F_{mj}. The superscript "u" of $G^u(s)$ is referred to the "uncut" condition. That is, milling process, shown in Fig. 6b, has not been engaged at all.

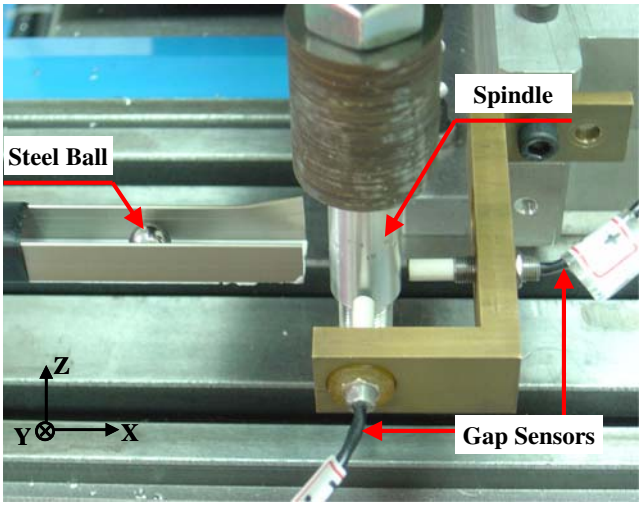

Fig. 8 Photo of impulse test

The test rig for obtaining the impulse response, shown in Fig. 7, includes the milling machine (Model CNC-K3 by How-mau Machinery Co., Ltd.), a pair of gap sensors (Model KD-2300.1SU by Kaman Instrumentation Corporation), and a particular auxiliary setup composed by a spring, a slot, and a steel bead. The steel bead is utilized to exert an impulse force upon the spindle along the direction of X-axis. The spindle position deviation due to the bead impact is continuously acquired by the gap sensors, shown in Fig. 8, and converted into electric voltage by the signal processing interface DS1104 by dSPACE. Eventually, the damping ratio, ζ, of spindle in X-direction can be calculated by the equation as follows [15]:

$$\frac{1}{n} \ln \frac{x_1}{x_2} = \frac{2\pi\xi}{\sqrt{1-\xi^2}} \quad (4)$$

Fig. 7 Test rig of the spindle modeling

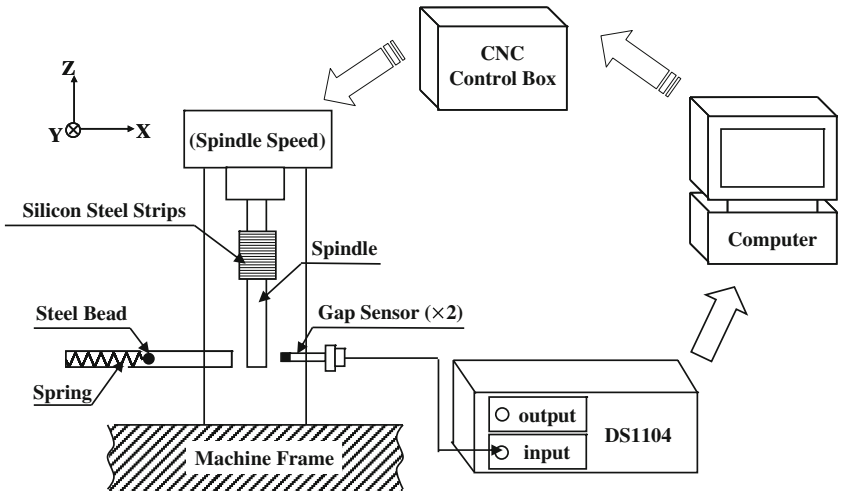

Table 1 Transfer functions of spindle against spindle speed

Spindle speed	Approximate damping ratio	Transfer function
Low speed (below 1,500 rpm)	0.0291	$\widetilde{G}^{u}_{xx} = \widetilde{G}^{u}_{yy} = \frac{50}{s^2+66.8s+1{,}210{,}869}$
	0.0326	$\widetilde{G}^{u}_{xy} = \widetilde{G}^{u}_{yx} = \frac{40}{s^2+111.46s+2{,}734{,}837}$
Medium speed (1,501–5,000 rpm)	0.0227	$\widetilde{G}^{u}_{xx} = \widetilde{G}^{u}_{yy} = \frac{60}{s^2+50.03s+1{,}210{,}869}$
	0.0265	$\widetilde{G}^{u}_{xy} = \widetilde{G}^{u}_{yx} = \frac{50}{s^2+87.65s+2{,}734{,}837}$
High speed (above 8,500 rpm)	0.0206	$\widetilde{G}^{u}_{xx} = \widetilde{G}^{u}_{yy} = \frac{90}{s^2+42.26s+1{,}210{,}869}$
	0.0244	$\widetilde{G}^{u}_{xy} = \widetilde{G}^{u}_{yx} = \frac{60}{s^2+80.7s+2{,}734{,}837}$

where x_1 and x_2 are two peaks of the recorded spindle position deviation. "$n-1$" is the number of peaks between x_1 and x_2

Based on the experimental data for damping ratio, evaluated by Eq. 4, by applying curve fitting method, the damping ratio can be estimated in terms of spindle speed, Ω, as follows:

$$\widetilde{\xi}_x(\Omega) = -6.4\,\Omega^{-1} + 0.678\,\Omega^{-0.5} + 0.0141 \tag{5}$$

$$\widetilde{\xi}_{xy}(\Omega) = -6.59\,\Omega^{-1} + 0.672\,\Omega^{-0.5} + 0.018 \tag{6}$$

where $\widetilde{\zeta}_x$ and $\widetilde{\zeta}_{xy}$ are the estimated damping ratio of spindle in X- and Y-axes, respectively.

Applying fast Fourier transform (FFT) technique, the frequency response of spindle under impulse excitation is pretty close to a second-order dynamic system. Therefore, the estimated transfer functions in Eq. 3 can be represented as follows:

$$\widetilde{G}^{u}_{xx}(s) = \widetilde{G}^{u}_{yy}(s) = \frac{K_1}{s^2 + 2\widetilde{\xi}_x\omega^{u}_n s + (\omega^{u}_n)^2} \tag{7}$$

$$\widetilde{G}^{u}_{xy}(s) = \widetilde{G}^{u}_{yx}(s) = \frac{K_2}{\left[s^2 + 2\widetilde{\xi}_{xy}\omega^{u}_n s + (\omega^{u}_n)^2\right]} \tag{8}$$

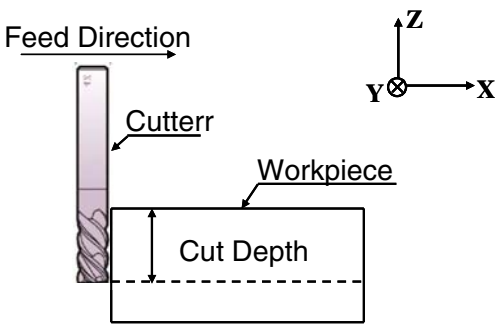

Fig. 9 Cutting test to record step response

where K_1 and K_2 are constants. ω^{u}_n is the natural frequency of spindle dynamics under "uncut" operation mode and retained unchanged no matter how the speed of spindle is tuned. It is noted that in this section, we have assumed that the spindle is perfectly symmetric and homogeneous in X- and Y-directions.

In order not to make the mathematic models complicated for synthesis of controller, the spindle speeds are divided into three categories: high speed, medium speed, and low speed. The corresponding transfer functions for Eqs. 7 and 8 are listed in Table 1. The top script "~" indicates that the transfer function is estimated by mathematical models. It is evident to notice that due to gyroscopic effect, the damping ratio is decreased as the spindle speed is increased.

Although two gap sensors are used in this work to measure the spindle position deviation in X- and Y-directions, in fact they can be replaced by self-sensing technique applied on AMB set [16] such that the cost and the additional space to equip a pair of gap sensors can be waived.

3.2 Modeling of milling dynamics

As aforesaid, the axial cut depth, a, mainly determines the patterns of cutting dynamics. Therefore, for spindle under

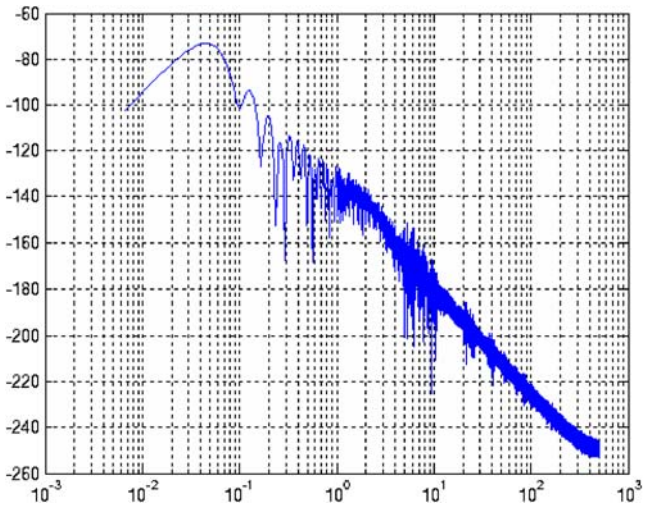

Fig. 10 Frequency response of spindle under step milling process

Table 2 Estimated system parameters in *X*-axis of spindle under milling

	Low spindle speed 3,500rpm	High spindle speed 7,000rpm
Low feed rate 150 mm/min	$\widetilde{\xi}_x^{\mathrm{L}} = 0.88525$	$\widetilde{\xi}_x^{\mathrm{hl}} = 0.60865$
	${}_x\widetilde{\omega}_n^{\mathrm{L}} = 0.3407$	${}_x\widetilde{\omega}_n^{\mathrm{hl}} = 2.6959$
High feed rate 300 mm/min	Unstable	$\widetilde{\xi}_x^{\mathrm{H}} = 0.49711$
		${}_x\widetilde{\omega}_n^{\mathrm{H}} = 182.44$

Unit of natural frequency: radians per second

cutting operation, shown in Fig. 6b, the dynamics can be represented as follows:

$$\begin{bmatrix} d_x \\ d_y \end{bmatrix} = G^{\mathrm{c}}(s) \begin{bmatrix} a_x \\ a_y \end{bmatrix} = \begin{bmatrix} G_{xx}^{\mathrm{c}}(s) & G_{xy}^{\mathrm{c}}(s) \\ G_{yx}^{\mathrm{c}}(s) & G_{yy}^{\mathrm{c}}(s) \end{bmatrix} \begin{bmatrix} a_x \\ a_y \end{bmatrix} \tag{9}$$

where d_x, d_y and a_x, a_y are the components of the spindle deviation, d, and axial cutting depth, a, in *X*- and *Y*-axes, respectively. $G^c(s)$ is the transfer function of spindle position deviation with respect to the axial cut depth. $G_{ij}^{\mathrm{c}}(s)(i = x,\ y\ ;\ \ j = x,\ y)$ represents the individual transfer function for system output, d_i, to the system input, a_j. It is noted that the superscript "*c*" in Eq. 9 is referred to "cutting operation".

The experimental rig for cutting tests mainly consists of the milling machine CNC-K3, a pair of gap sensors, and a milling cutter, with diameter 6 mm and four cutting blades. The cutting path, shown in Fig. 9, is designed to record the step response of the spindle position deviation. The axial cut depth is 1 mm. Totally, 24 milling tests have been undertaken under various spindle speeds and feed rates.

The frequency response can be obtained by FFT and shown in Fig. 10. It is noted that an additional integrator "1/*s*" is embedded in Fig. 10 obtained by FFT since a step response is recorded, instead of impulse response. Therefore, the dynamics of spindle under milling can be regarded as a second-order system and the components of the transfer function matrix in Eq. 9 are represented as follows:

$$G_{xx}^{\mathrm{c}}(s) = G_{yy}^{\mathrm{c}}(s) = \frac{K_3}{s^2 + 2\xi_x^{\mathrm{c}}\left({}_x\omega_n^{\mathrm{c}}\right)s + \left({}_x\omega_n^{\mathrm{c}}\right)^2} \tag{10}$$

$$G_{xy}^{\mathrm{c}}(s) = G_{yx}^{\mathrm{c}}(s) = \frac{K_4}{s^2 + 2\xi_{xy}^{\mathrm{c}}\left({}_{xy}\omega_n^{\mathrm{c}}\right)s + \left({}_{xy}\omega_n^{\mathrm{c}}\right)^2} \tag{11}$$

where ζ_x^{c} and ζ_{xy}^{c} are the damping ratios of the spindle under milling in principle axis (i.e., *X*-direction) and the cross axis (i.e., *Y*-direction). ${}_x\omega_n^{\mathrm{c}}$ and ${}_{xy}\omega_n^{\mathrm{c}}$ are the associated natural frequencies. K_3 and K_4 are constants.

The system parameters ζ_x^{c}, ζ_{xy}^{c}, ${}_x\omega_n^{\mathrm{c}}$, and ${}_{xy}\omega_n^{\mathrm{c}}$ can be evaluated from the recorded step response by the following equations [17]:

$$M_{\mathrm{o}} = e^{-\pi\xi/\sqrt{1-\xi^2}} \tag{12}$$

$$t_{\mathrm{r}} \approx \frac{1.8}{\omega_n} \tag{13}$$

where M_{o} is the maximum overshoot and t_{r} is the rise time. Based on intensive experiments, the damping ratios and natural frequencies can be estimated in terms of spindle speed, Ω, and feed rate, f, as follows:

$$\widetilde{\xi}_x^{\mathrm{c}}(f,\ \Omega) = 0.351f^{-0.1} + 13.802\Omega^{-0.6} + 0.299 \tag{14}$$

$$\widetilde{\xi}_{xy}^{\mathrm{c}}(f,\ \Omega) = 0.279f^{-0.1} + 5.882\Omega^{-0.6} + 0.161 \tag{15}$$

$${}_x\widetilde{\omega}_n^{\mathrm{c}}(f,\ \Omega) = 0.0225f + 0.0002\Omega - 0.3467 \tag{16}$$

$${}_{xy}\widetilde{\omega}_n^{\mathrm{c}}(f,\ \Omega) = 0.0431f + 0.0006\Omega - 1.023 \tag{17}$$

where $\widetilde{\xi}_x^{\mathrm{c}}$ and $\widetilde{\xi}_{xy}^{\mathrm{c}}$ are the estimated damping ratios. ${}_x\widetilde{\omega}_n^{\mathrm{c}}$ and ${}_{xy}\widetilde{\omega}_n^{\mathrm{c}}$ are the estimated natural frequencies. It is noted that the coefficients in Eqs. 14–17 are obtained by curve fitting method.

In order to simplify the representation of spindle model under milling operation so that the controller can be easier to be synthesized, the patterns of feed rate and spindle speed are both categorized into two types: "low feed rate/high federate" and "low spindle speed/high spindle speed", respectively. The estimated system parameters are listed in

Table 3 Estimated system parameters in *Y*-axis of spindle under milling

	Low spindle speed 3,500rpm	High spindle speed 7,000rpm
Low feed rate 150 mm/min	$\widetilde{\xi}_{xy}^{\mathrm{L}} = 0.50527$	$\widetilde{\xi}_{xy}^{\mathrm{hl}} = 0.38739$
	${}_{xy}\widetilde{\omega}_n^{\mathrm{L}} = 0.40699$	${}_{xy}\widetilde{\omega}_n^{\mathrm{hl}} = 5.3863$
High feed rate 300 mm/min	Unstable	$\widetilde{\xi}_{xy}^{\mathrm{H}} = 0.29855$
		${}_{xy}\widetilde{\omega}_n^{\mathrm{H}} = 335.23$

Unit of natural frequency: radians per second

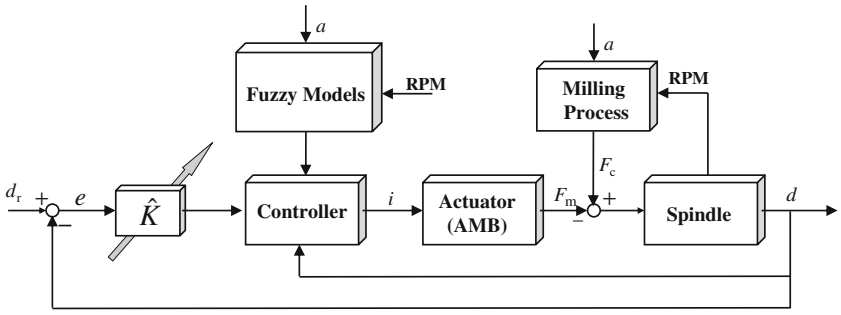

Fig. 11 Block diagram of self-tuning fuzzy control system

Tables 2 and 3 accordingly, where the superscripts of estimated damping ratios and estimated natural frequencies are denoted as "L" and "H" to indicate which operation condition is referred to. For example, $\widetilde{\xi}_x^{\mathrm{hl}}$ is referred to the estimated damping ratio for high spindle speed and low feed rate in X-axis.

4 Self-tuning fuzzy logic control for milling process

The block diagram of self-tuning fuzzy control system is shown in Fig. 11. In this work, the fuzzy models, to be defined later, are constructed in order to on-line estimate the cutting force, F_c. Once the estimated cutting force, $\widehat{F}_c$,, is obtained, the compensatory magnetic force, F_m, can be determined to counterbalance F_c, i.e., $F_m = -\widehat{F}_c$. In addition, a self-tuning adaptive gain, $\widehat{K}$, is proposed to regulate the spindle position regulation as follows:

$$\dot{\widehat{K}} = \widehat{K}|d_r - d| \tag{18}$$

where d_r is the nominal air gap. The required coil current to generate the compensatory force can be determined by Eq. 1.

4.1 Fuzzy model for spindle dynamics

The so-called fuzzy model of spindle dynamics in this paper is referred to three spindle speed grades: high speed, medium speed, and low speed. It is noted that the natural frequency remains unchanged with respect to spindle speed. On the other hand, the fuzzy damping ratio can be described as follows:

$$\widehat{\xi}_x^{\mathrm{u}} = \mathrm{W}_\xi^{\mathrm{L}}\widetilde{\xi}_x^{\mathrm{L}} + \mathrm{W}_\xi^{\mathrm{M}}\widetilde{\xi}_x^{\mathrm{hl}} + \mathrm{W}_\xi^{\mathrm{H}}\widetilde{\xi}_x^{\mathrm{H}} \tag{19}$$

$$\widehat{\xi}_{xy}^{\mathrm{u}} = \mathrm{W}_\xi^{\mathrm{L}}\widetilde{\xi}_{xy}^{\mathrm{L}} + \mathrm{W}_\xi^{\mathrm{hl}}\widetilde{\xi}_{xy}^{\mathrm{hl}} + \mathrm{W}_\xi^{\mathrm{H}}\widetilde{\xi}_{xy}^{\mathrm{H}} \tag{20}$$

where $\mathrm{W}_\xi^{\mathrm{L}}$, $\mathrm{W}_\xi^{\mathrm{M}}$, and $\mathrm{W}_\xi^{\mathrm{H}}$ are the corresponding weighting coefficients whose membership functions are defined in Fig. 12. $\overline{\Omega}$ is the normalized spindle speed by 8,500 rpm.

4.2 Fuzzy model for spindle dynamics under cutting operation

Unlike the idle operation mode, the natural frequencies of the spindle dynamics under cutting operation, though still independent of spindle speed, are altered by various feed rate and cut depth. By the same arguments in Section 4.1, the fuzzy system parameters for spindle dynamics under cutting operation mode can be described as follows:

$$\widehat{\xi}_x^{\mathrm{c}} = \mathrm{W}_\xi^{\mathrm{L}}\widetilde{\xi}_x^{\mathrm{L}} + \mathrm{W}_\xi^{\mathrm{hl}}\widetilde{\xi}_x^{\mathrm{hl}} + \mathrm{W}_\xi^{\mathrm{H}}\widetilde{\xi}_x^{\mathrm{H}} \tag{21}$$

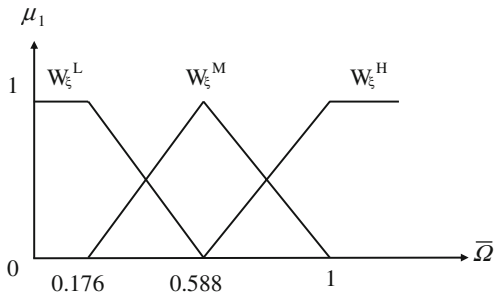

Fig. 12 Membership functions for fuzzy model of spindle dynamics

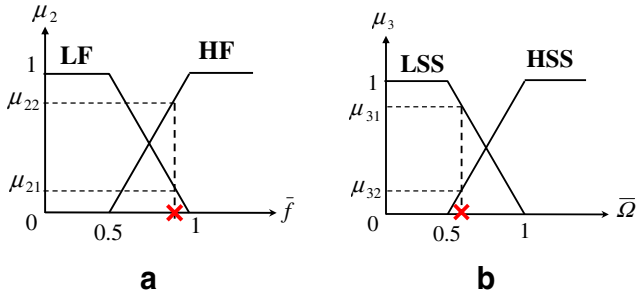

Fig. 13 Membership functions due to **a** feed rate and **b** spindle speed

Table 4 Weighting coefficients for fuzzy model under milling mode

$\frac{\overline{\Omega}}{\overline{f}}$	μ_{31}	μ_{32}
μ_{21}	μ_{I}	μ_{II}
μ_{22}		μ_{III}

$$ {}_x\widehat{\omega}_n^{\mathrm{c}} = \mathrm{W}^{\mathrm{L}}_{\omega_n\, x}\widetilde{\omega}_n^{\mathrm{L}} + \mathrm{W}^{\mathrm{hl}}_{\omega_n\, x}\widetilde{\omega}_n^{\mathrm{hl}} + \mathrm{W}^{\mathrm{H}}_{\omega_n\, x}\widetilde{\omega}_n^{\mathrm{H}} \tag{22} $$

$$ \widehat{\xi}^{\mathrm{c}}_{xy} = \mathrm{W}^{\mathrm{L}}_{\xi}\widetilde{\xi}^{\mathrm{L}}_{xy} + \mathrm{W}^{\mathrm{hl}}_{\xi}\widetilde{\xi}^{\mathrm{hl}}_{xy} + \mathrm{W}^{\mathrm{H}}_{\xi}\widetilde{\xi}^{\mathrm{H}}_{xy} \tag{23} $$

$$ {}_{xy}\widehat{\omega}_n^{\mathrm{c}} = \mathrm{W}^{\mathrm{L}}_{\omega_n\, xy}\widetilde{\omega}_n^{\mathrm{L}} + \mathrm{W}^{\mathrm{hl}}_{\omega_n\, xy}\widetilde{\omega}_n^{\mathrm{hl}} + \mathrm{W}^{\mathrm{H}}_{\omega_n\, xy}\widetilde{\omega}_n^{\mathrm{H}} \tag{24} $$

The membership functions for the normalized feed rate, $\overline{f}$, and spindle speed, $\overline{\Omega}$, are shown in Fig. 13, where the abbreviations PS and PB indicate "positive small" and "positive big", respectively. Similarly, the feed rate and spindle speed are normalized by maximum values shown in Tables 2 and 3, respectively. The weighting coefficients in Eqs. 21–24 are determined by μ_{I}, μ_{II}, and μ_{III} in Table 4, where the minimum defuzzification rule is employed.

4.3 Experiments on milling process under self-tuning fuzzy control

The profile of acrylic workpiece for milling is depicted in Fig. 14, including six regions. The dotted line in Fig. 14 is the cutting path to be undertaken. That is, the cutting force is faced with various resistances in the forms of step, ramp, and circular arc during milling process. The operation conditions for milling tests are set as

(a) Spindle speed 7,500 rpm, feed rate 120 mm/min
(b) Spindle speed 2,000 rpm, feed rate 240 mm/min

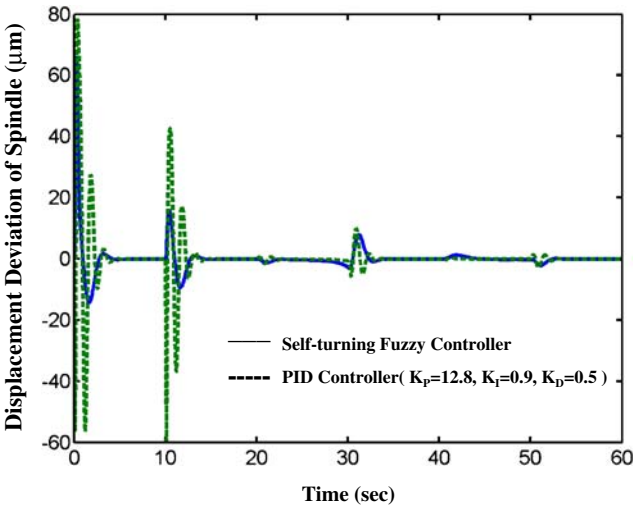

Fig. 15 Spindle position deviation (spindle speed 7,500 rpm, feed rate 120 mm/min)

(c) Spindle speed 2,000 rpm, feed rate 240 mm/min but the cut depth is increased by 0.5 mm. That is, the dotted line in Fig. 14 is lowered down by 0.5 mm.

Since the fuzzy damping ratio and natural frequency for milling process are available by fuzzy models, the dynamic cutting force for the cutting test specified by Fig. 14 can be estimated by the on-line measurement of spindle position deviation and its derivatives. In order to verify the validity of the cutting force estimation by fuzzy controller, a dynamometer (Model: 9254, by Kistler) is utilized as the benchmark.

In order to verify the superiority of the proposed self-tuning fuzzy controller, the spindle position deviations under conventional PID control law are also shown in Figs. 15, 16, and 17. It is evident to observe that the overshoots under self-tuning fuzzy controller are relatively

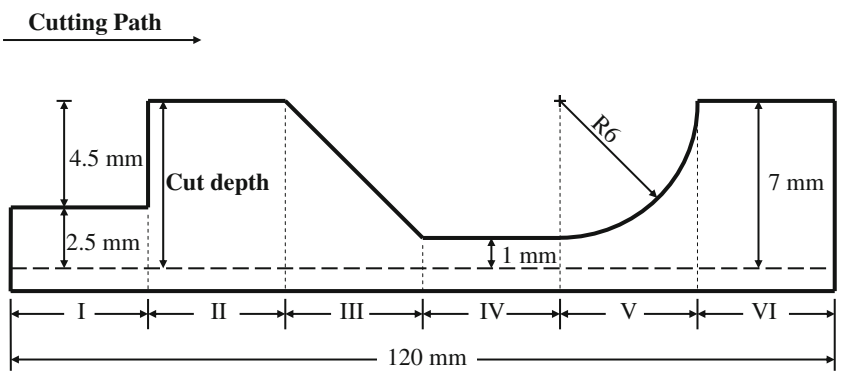

Fig. 14 Profile of workpiece for milling test

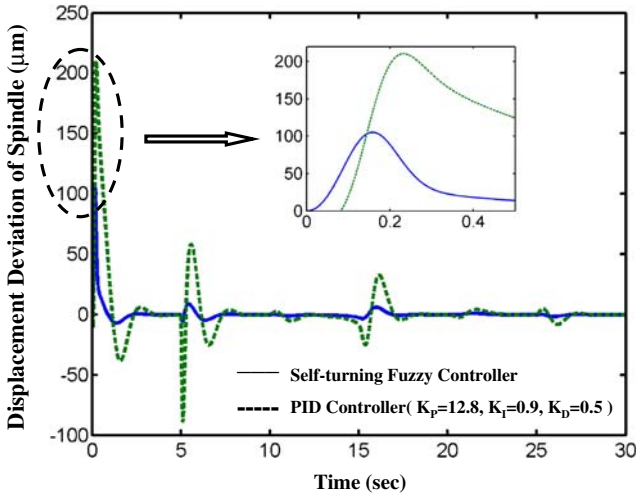

Fig. 16 Spindle position deviation

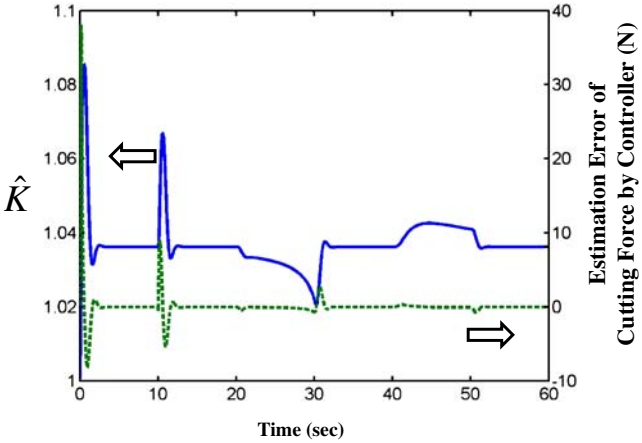

Fig. 18 Self-tuning adaptive gain and estimation error of cutting force in *X*-axis by self-tuning fuzzy controller (spindle speed 7,500 rpm, feed rate 120 mm/min)

limited while the overshoots under PID controller become at least 200%, especially for harsh milling condition (i.e., low spindle speed but high federate or large cut depth). Besides, the self-tuning fuzzy controller exhibits to be able to adjust its feedback gain fairly quick once the cut depth is suddenly altered, i.e., the corners between any two intervals of cutting path shown in Fig. 14. On the other hand, the estimation error of cutting force and the adaptive control gain, $\hat{K}$, by the fuzzy controller is recorded, compared with the measure by the dynamometer and shown in Fig. 18. It is noted that the worst estimations by the fuzzy controller occur at the intersections of any two adjacent regions where the patterns of cut depth are drastically changed.

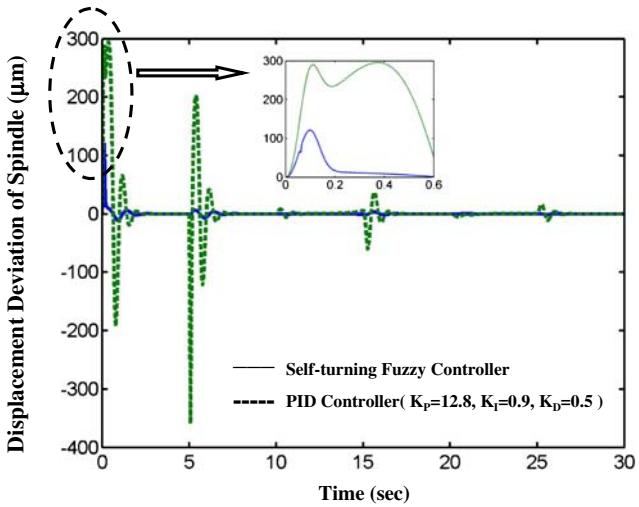

Fig. 17 Spindle position deviation (spindle speed 2,000 rpm, feed rate 240 mm/min, cut depth increased by 0.5 mm)

5 Conclusions

Conventionally, the spindle position deviation can be regulated by a simple feedback loop, e.g., PID action or linear quadratic regulation (LQR). However, the root cause which provokes the spindle position deviation, i.e., cutting force, is not suppressed at all either by PID or LQR. Furthermore, the chatter phenomenon might be emerged as long as the cutting force is not appropriately counterbalanced. An embedded AMB is designed, presented, and equipped with the milling machine to provide the required the counterbalance force in this paper. The cutting force during milling process is estimated by the proposed fuzzy controller which is based on the fuzzy dynamic models, obtained by experiments, and the on-line measurement of spindle position deviation. Since the damping ratio and the natural frequency of the milling dynamic are slightly altered by spindle speed and federate, respectively, the dynamic milling process can be fuzzified into a few submodels.

The fuzzy controller is verified by intensive milling tests for its efficacy of counterbalance upon cutting force and capability of spindle position regulation via the embedded AMB. The required coil current applied to the AMB is determined by the estimation of cutting force and the on-line measurement of spindle position deviation. It has been noticed that the worst estimation of cutting force by the proposed fuzzy logic algorithm occurs at the intersection of any two adjacent patterns of expected profile of the workpiece to be milled.

Acknowledgement This research was supported by *National Science Council* (Taiwan) under Grants 97-2221-E-006-182. The authors would like to express their appreciation.

References

1. Park SS, Qin YM (2007) Robust regenerative chatter stability in machine tools. Int J Adv Manuf Technol 33(3–4):389–402
2. Lauderbaugh LK, Ulsoy AG (1988) Dynamic modeling for control of milling process. J Eng Ind 110(4):367–375
3. Li HZ, Li XP, Chen XQ (2003) A novel chatter stability criterion for the modeling and simulation of the dynamic milling process in the time domain. Int J Adv Manuf Technol 22(9–10):619–625
4. Yang MY, Lee TM (2002) Hybrid adaptive control based on the characteristics of CNC end milling. Int J Mach Tools Manuf 42:489–499
5. Peng YH (2004) On the performance enhancement of self-tuning adaptive control for time-varying machining processes. Int J Adv Manuf Technol 24(5):395–403
6. Nolzen H, Isermann R (1995) Fast adaptive cutting force control for milling operation. IEEE Conference on Control Applications, pp 760–765
7. Jee S, Koren Y (2004) Adaptive fuzzy logic controller for feed drives of a CNC machine tool. Mechatronics 14(3):299–326
8. Liu Y, Wang C (1999) Neural network based adaptive control and optimization in the milling process. Int J Adv Manuf Technol 15 (11):791–795
9. Spirig M, Schmied JP, Kanne U (2002) Three practical examples of magnetic bearing control design using a modern tool. J Eng Gas Turbine Power 124(4):1025–1031
10. Kyung JH, Lee CW (2003) Controller design for a magnetically suspended milling spindle based on chatter stability analysis. JSME International Journal, Series C 46(2):416–422
11. Allaire PE, Humphris RR, Kelm RD (1985) Dynamics of a digitally controlled magnetic bearing. Nippon Kikai Gakkai Ronbunshu 51(465):1095–1100
12. Tsai N-C, Kuo C-H, Lee R-M (2007) Regulation on radial position deviation for vertical AMB systems. Mech Syst Signal Process 21:2777–2793
13. Tsai N-C, Hsu S-L (2007) On sandwiched magnetic bearing design. Electromagnetics 27(6):371–385
14. Neff HP (1987) Basic electromagnetic fields, 2nd edn. Harper & Row, New York
15. Kuo BC (1997) Automatic control systems, 7th edn. Prentice Hall, New Jersey
16. Tsai N-C, Huang W-M, Chiang C-W (2008) Dynamic analysis of magnetic actuator for micro-gyroscopes. Electromagnetics 29 (2):105–124
17. Franklin GF, Powell JD, Abbas EN (1994) Feedback control of dynamics systems, 3rd edn. Addison Wesley, New York